Experimental study of a radial plasma source

G. Makrinich and A. Fruchtman
H.I.T.–Holon Institute of Technology, 52 Golomb Street, Holon 58102, Israel

(Received 9 February 2009; accepted 25 March 2009; published online 23 April 2009)

A radially outward acceleration of plasma in cylindrical geometry along an applied electric field and across an axial magnetic field is studied. The configuration, coined a radial plasma source, consists of two ceramic disks positioned parallel to each other, between which a cylindrical molybdenum anode is mounted. The electric field is generated by applying a voltage between the anode and a heated cathode neutralizer that is located away from the ceramic disks. The plasma diagnostic system includes Langmuir probes, an emissive probe, and a balance force meter. The discharge voltage is found to increase when the magnetic field is increased or when the mass flow rate (and the pressure) is decreased. For a discharge current of 1.4 A, the discharge voltage increases from 55 to 120 V when the magnetic field is increased from 0 to 186 G. The azimuthal uniformity of the plasma flow is found to decrease with the increase in gas pressure. The force exerted on the balance force meter is found to be larger than the force exerted by the plasma flow. This disparity indicates that a considerable part of the force is exerted by the neutral gas, which has gained momentum from the plasma via ion-neutral collisions. The force is increased because the momentum delivered for a given deposited power is larger if the energy is deposited in a larger mass, as happens here through plasma collisions. We estimate theoretically the expected force at the collisionless and the collisional limits and find that the measured force is between the expected forces at the two limits. © *2009 American Institute of Physics*. [DOI: 10.1063/1.3119688]

I. INTRODUCTION

Ion flux and the force exerted by the plasma flow are important for the characterization of flowing-plasma sources. A better understanding of the generation of the ion flux and the exerted force can improve various technological processes such as plasma surface treatment and plasma propulsion. We have designed a plasma source of a cylindrical geometry with an applied axial magnetic field in order to generate a radially outward ion flow. To that end the inner part of the source is biased positively (as the anode). Cylindrical plasma sources with a radial flow are often being studied and used.[1–5] To allow an uninterrupted radial flow of the plasma, we do not employ an annular cathode in our radial plasma source (RPS), but rather a cathode that is a thin cylindrical rod located parallel and at a distance from the source axis. This cathode is similar to the neutralizer used, for example, in the Hall thruster.[6] The dynamics of the plasma is also expected to have similarities to that in the Hall thruster; the electron inward radial motion is impeded by the magnetic field, so that the electrons have a large azimuthal $E \times B$ drift, as in the Hall thruster. Here E and B are the electric and the magnetic fields. Since propellant saving is crucial, Hall thrusters rely on an almost full ionization of the propellant.[6] However, for other uses, where energy saving is more important, delivering of thrust through a partially ionized plasma might be advantageous.[7–9] Also, the use of partially ionized plasma becomes necessary when one might encounter the need for propulsion in a millitorr pressure environment.

In our work we will examine the influence of mutual collisions between a neutral gas of a millitorr pressure and the generated plasma on the plasma flow and the force exerted by the flow. The measurements were carried out in argon gas plasmas for different ambient gas pressures and magnetic field intensity up to 0.02 T. We measured the discharge applied voltage and current, ion saturation currents into a probe, the plasma potential, and the force exerted on a balance force meter. The balance force meter has been designed so that it measures the force exerted on it by the flowing plasma and neutrals with an accuracy of 10%.

The azimuthal uniformity of the ion radial flux was found to decrease with the increase in gas pressure. Most of the applied voltage was found to drop in the vicinity of the anode where the axial magnetic field is applied. The measured force exerted on the balance force meter by plasma flow is larger than the force calculated with the assumption that it is all exerted by the ions. The source of the larger measured force could be ion collisions with neutrals that result in a larger total force exerted by both ions and neutrals.

In Sec. II we describe the experimental setup, the design of the RPS, and the measurement system. In Sec. III we describe the measurements of the plasma parameters. The force measurements are presented and discussed in Sec. IV. We conclude in Sec. V.

II. THE EXPERIMENTAL SETUP

A. Plasma source

The RPS, shown in Fig. 1, with a schematic of the electric circuit, consists of a ceramic unit, a molybdenum anode, a magnetic-field generating solenoid, an iron core, a gas distributor, and a cathode. The ceramic unit is composed of two annular disks connected with an axial segment. The outer diameter of each of the annular disks is 77 mm, the inner

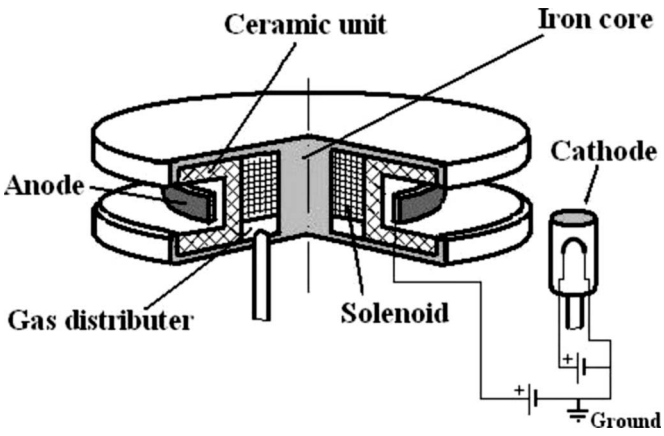

FIG. 1. The RPS with a schematic of the electric circuit.

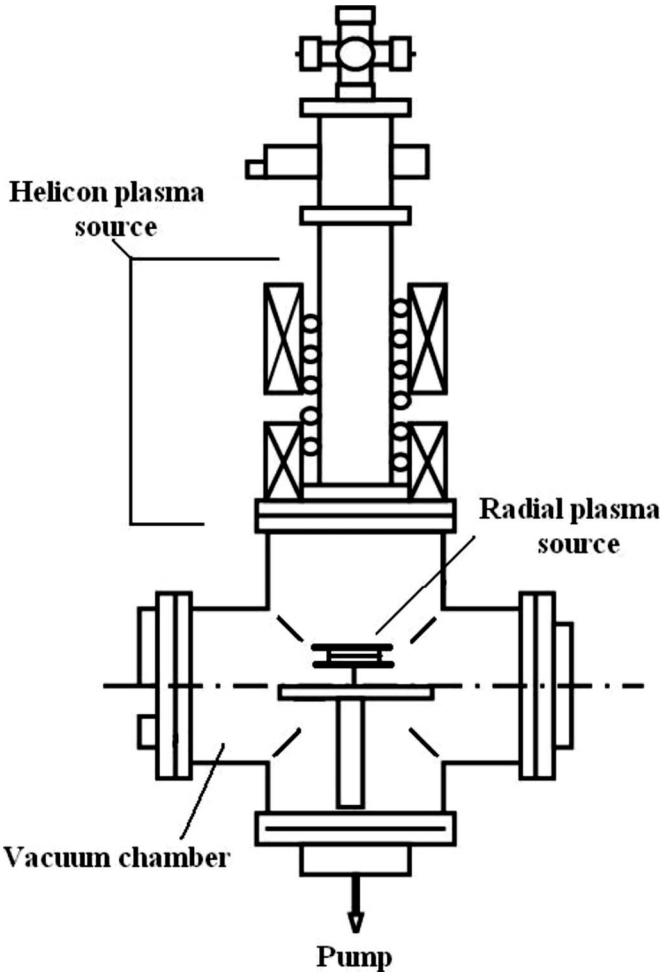

FIG. 2. The experimental system.

diameter is 30 mm, and the axial distance between the two disks is 5 mm. The molybdenum cylindrical anode is of 48 mm in diameter, 4.5 mm in height, and 0.25 mm in thickness. Together with the iron core, the solenoid generates a magnetic field that is concentrated at the outer edge of the source. For a current in the solenoid of 4 A the generated magnetic field at the edge is 0.02 T. As is seen in the figure, the ceramic unit, the solenoid, and the iron core have the same axis of symmetry. The empty cylindrical volume between those three parts (see the figure) plays a role of a gas distributor, through which the working gas is supplied through holes in the ceramic unit into the space between the two annular disks. The mass flow rate is varied from 17.5 to 50 SCCM (SCCM denotes cubic centimeter per minute at STP) argon gas and, consequently, the pressure in the vacuum chamber changes from 2.5 to 6.6 mTorr. For neutralizing the ion-flow current we employ a cathode neutralizer located 40 mm from the outer edge of the source. The electron emission is achieved by heating a tungsten five-turn loop of 10 mm in diameter and 15 mm in height by a dc current of 19 A. For reducing the heating of other parts of the source, the loop is positioned inside a molybdenum cylinder of 25 mm in diameter, 45 mm in height, and 0.25 mm in thickness. An argon gas of 4 SCCM mass flow rate flows through the cathode.

As is shown in Fig. 2, the RPS is located at the center of a cross ISO 320 vacuum chamber. The vacuum chamber is pumped to a base pressure of 0.01 mTorr by a two-stage pump station that consists of a mechanical pump and a turbomolecular pump. The vacuum chamber is equipped with pressure measurement gauges and two mass flow rate meters. The adjacent helicon plasma source is used for an easier ignition of the dc discharge in the RPS.

There are two ways to ignite the source. We may employ the helicon source for generating dilute plasma around the RPS and then ignite it by heating the cathode (with driving a 19 A heating current through the cathode) and applying a voltage between the anode and the cathode. When the RPS is ignited we switch off the helicon source. Alternatively, instead of employing the helicon source, we employ a larger heating current of 22 A through the cathode while we apply the voltage between the anode and the cathode. When the source is ignited the heating current is decreased to 19 A.

In the experiments we observed a strong effect of the magnetic field. When there is no magnetic field, the discharge was highly nonuniform azimuthally and occupied only a part of the volume of the ceramic unit. The plasma is of a ball shape (see Fig. 3) and is somewhat similar to other plasma balls excited near a positive electrode.[10,11] The discharge in the absence of a magnetic field will be described in another paper. In this paper we do not investigate the operation of the RPS when the magnetic field is zero. In the presence of the magnetic field the discharge occupies all the volume in the ceramic unit. The plasma has an annular shape because the electrons are expected to have a large azimuthal $E \times B$ drift. The plasma ions, on the other hand, are assumed to be accelerated radially outward. For a constant discharge current, the increase in the intensity of the axial magnetic field results in an increase in the voltage between the anode and the cathode. Figure 4 shows the plasma filling the space between the disks during this operation mode of the RPS with a magnetic field. Also in both Figs. 3 and 4 are marked the balance force meter (the dark flat plate in the left part of the picture) and the cathode (in the right part of the picture). The balance force meter will be described in subsection II B.

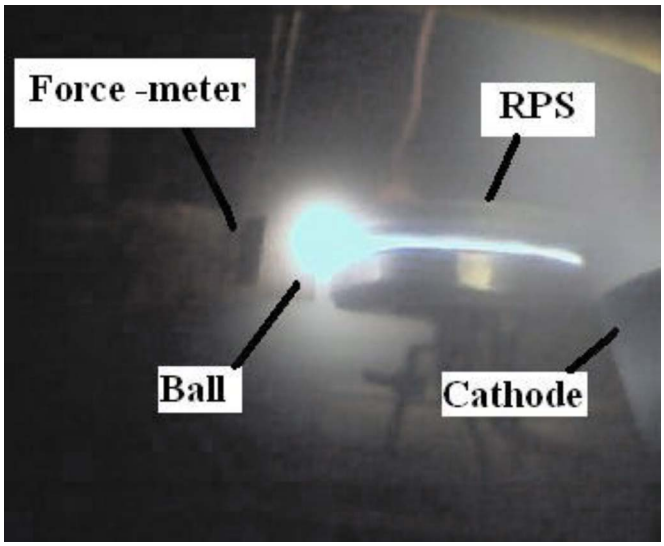

FIG. 3. (Color online) The RPS operation in the absence of a magnetic field.

B. Measurement system

The system for measuring the local plasma flow parameters consists of three different parts: a balance force meter, a flat Langmuir probe, and a floating emissive probe. The flat Langmuir probe is employed for measuring the ion particle flux flowing from the RPS. The floating emissive probe is employed for measuring the local plasma potential. The balance force meter is used for measuring the force exerted by the flow.

The balance force meter is presented schematically in Fig. 5. Other instruments to measure the force on a target plate employ strain gauges[8] or capacitance manometers.[12] Our balance force meter used torque balance between different forces. The balance force meter, made of mica, is a flat plate of dimensions 17.5×21.5 mm^2, a 0.08 mm thickness, and a mass of 0.075 g. The plate is positioned on two aluminum bars of 0.25 mm in diameter. The distance between the bars is 15 mm. In the top part, the balance force meter has two equal-mass arms, where h, the distance from the axis, is $h=16$ mm. The arms are used for the balance force-meter calibration. The length of the balance force meter from the axis of rotation to the lower edge of the flat plate is $k=119$ mm. The balance force meter rotates on tungsten of 0.25-mm-diameter axis lubricated by disulfide molybdenum.

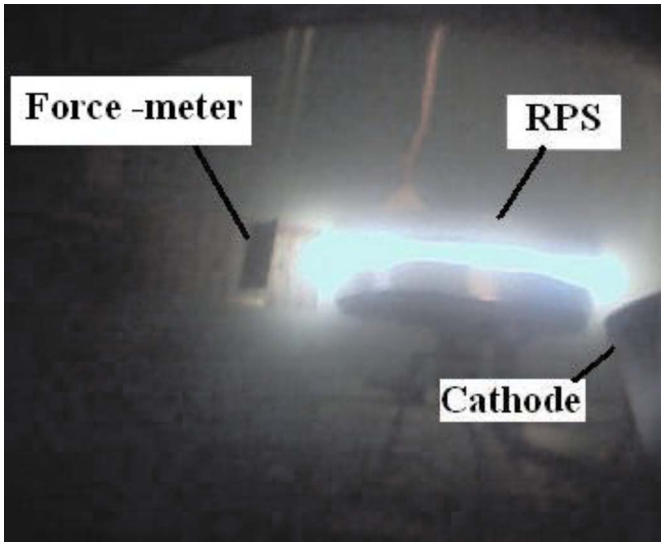

FIG. 4. (Color online) The RPS operation in the presence of a magnetic field.

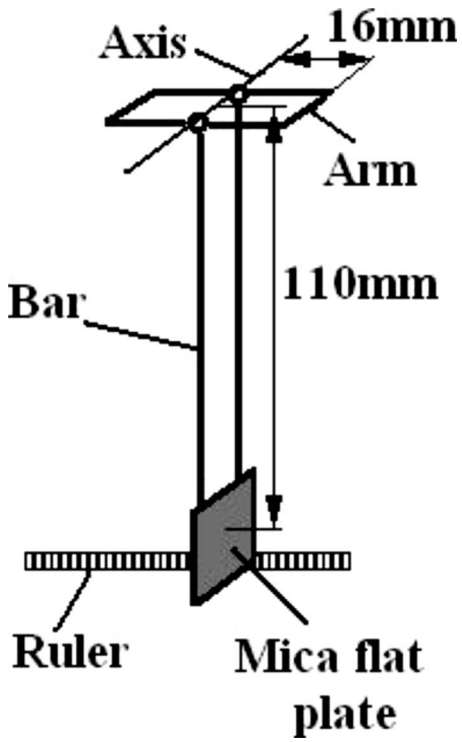

FIG. 5. The balance force meter.

When the plasma and gas impinge on the flat plate, the plate and the bars rotate relative to the vertical axis with an angle α. At this angle the sum of the torques of the force exerted by the plasma and gas impinging on the plate and of the gravitational force is zero. Relative to the axis of rotation, the torque of F, the (assumed horizontal) force by the flow (of plasma and gas), is $FL\cos\alpha$, where L is the distance between the plate center and the axis of the balance ($L=110$ mm in our meter). The torque of the gravitational force is $MgH\sin\alpha$, where M is the mass of the balance force meter, H is the distance between the axis of rotation and the center of mass of the balance force meter ($M=0.106$ g and $H=96$ mm in our meter), and g is the gravitation acceleration 9.81 m/s^2. Since the total torque is zero we find that F_{ex}, the force deduced from the measurements, is

$$F_{ex} = \frac{H}{L} Mg \tan\alpha. \quad (1)$$

The deviation angle was calculated from relation

$$\sin\alpha = \frac{l}{k}, \quad (2)$$

where l is a deviation length measured by the ruler (see Fig. 5) with a 0.25 mm accuracy.

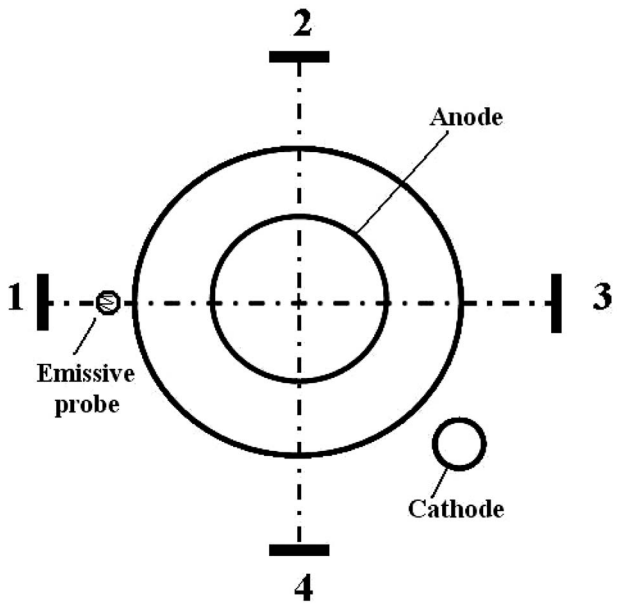

FIG. 6. The probe locations denoted as 1, 2, 3, and 4. The balance force meter while employed is positioned at the location denoted as 1. Also shown is the location of the emissive probe.

In order to estimate the error in the evaluation of F due to friction and deformation of the bars, we performed a calibration of the balance force meter. The calibration was done by employing masses that have been measured accurately (accuracy of 10^{-4} g). One of the arms of the balance force meter shown in Fig. 5 was loaded by the masses. As a result the flat plate and the bars rotated with an increasing deviation angle for an increased load weight. The deviation length l was measured as function of the mass. The best-fitted measured slope of the obtained curve that was found to be $a=201$ m/kg was compared with the calculated slope from the balance parameters $a=hk/HM=186$ m/kg. The difference between the two slopes was obtained as 8% of the calculated slope value. The good agreement between the two slopes indicates that the measurement by the balance force meter is very accurate. If we take into account additional error sources (the inaccuracy of l and k measurements), we conclude that the measurement of the force has 10% inaccuracy.

The floating emissive probe provides a direct plasma potential measurement. The emitting part of the probe is a 0.25-mm-diameter tungsten wire twisted into a three-turn loop 4 mm in diameter and 5 mm in length. The floating emissive probe is located at a distance of 1 cm from the outer edge of the plasma source (denoted in Fig. 6). The condition for the employment of the floating emissive probe is given in Refs. 13 and 14 as $B \ll 4.8T_e^{1/2}/d$, where B is magnetic field intensity (G), T_e is electron temperature (eV), and d is wire diameter (cm). For our argon plasma $T_e=3$ eV and wire diameter $d=0.025$ cm the condition becomes $B \ll 330$ G. The maximal magnetic field at the probe location is 30 G and therefore the use of the probe is justified.

For measuring the plasma potential we drove a current through the wire of the emissive probe of up to 7 A and measured the probe potential with respect to ground. The plasma potential is the probe potential when it is saturated. The probe potential was measured at saturation once with respect to the ground (or the cathode) and then with respect to the anode. The difference between the two measured probe potentials was found to be almost identical to the applied voltage between the anode and the cathode ($<4\%$). The good agreement indicates that the effect of leakage current is negligible.

The flat two-sided Langmuir probe was used for ion saturation current measurements. The molybdenum Langmuir probe is of dimensions 18.5×18.2 mm^2 and thickness of 0.25 mm. All measurements of the ion saturation current were taken at a small negative potential, -10 V relative to ground. We measured the ion saturation current in three situations. We call a perpendicular ion current I_{per} the ion saturation current into both sides of the probe when the plasma flow (assumed to be radially outward) is perpendicular to the probe surface. We then call a parallel ion current I_{par} the ion saturation also into both sides of the probe, but when the plasma flow is parallel to the probe surface. Finally, we call a downstream ion current I_{dn} the ion saturation current into the backside of the probe (facing downstream) when the plasma flow is perpendicular to the probe surface.

For the downstream ion current measurements, the upstream side of the probe area was isolated from the plasma flow by positioning on it an equal-area mica plate. The probe can then collect ions only from the downstream part of the flow. To determine the effect of leakage current to the upstream side beneath the mica plate, the upstream ion saturation current was measured separately. The sum of the separate upstream and downstream ion saturation currents was compared with the ion current when both sides are exposed and was found to be identical up to 5%.

III. PLASMA FLOW CHARACTERISTICS

In this section we describe several measurements of the plasma and the electric potential in the RPS. These measurements provide us with the ion saturation currents at several positions located at different azimuthal angles around the source, the discharge voltage, and the potential at the exit from the source, all as functions of the intensity of the magnetic field.

The measurements of the ion saturation currents at several positions located at the exit from the source indicate how azimuthally uniform the radial plasma flux is. The perpendicular ion current is measured at four positions located at a distance of 8 cm from the axis of symmetry of the RPS at an angle of 90° between each two lines connecting two neighboring positions with the center of the RPS. The locations of the four probes are denoted in Fig. 6 as 1, 2, 3, and 4. The perpendicular ion current at point j ($j=1$, 2, 3, or 4), $I_{per,j}$, is measured as a function of the varied mass flow rate of the gas that is injected through the ceramic unit. The measurements were performed for a constant magnetic field intensity whose maximal value across the center plane of the ceramic unit at the outer edge of the source is 136 G and for a discharge current of 1.4 A. These measurements presented

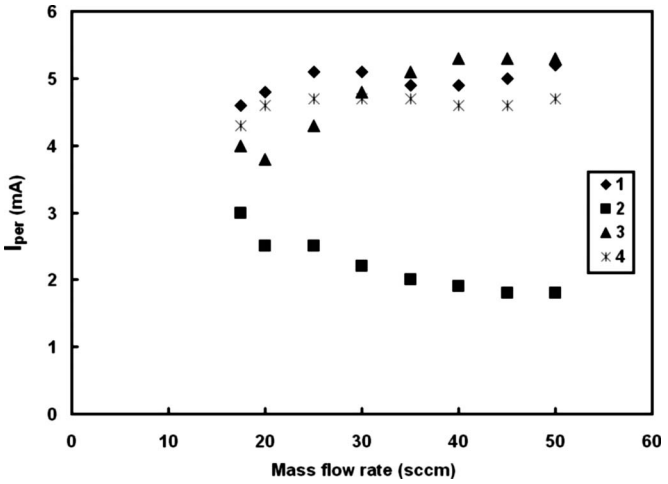

FIG. 7. The perpendicular ion current measured by the probes at the four locations shown in Fig. 6 as a function of the mass flow rate.

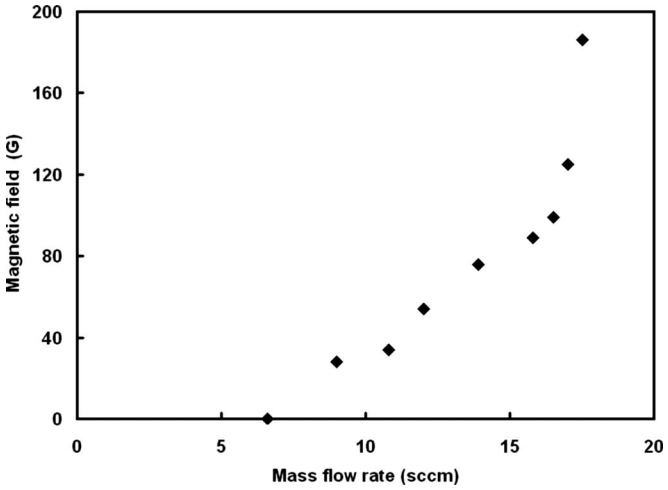

FIG. 9. The maximal magnetic field intensity for which the discharge is stable as a function of the mass flow rate. Also, the minimal mass flow rate for a specified magnetic field intensity for which the discharge is stable.

in Fig. 7 show that the azimuthal uniformity of the ion saturation decreases with the increase in the mass flow rate. The decrease probably follows the more often interruption of the azimuthal $E \times B$ electron drift by electron-neutral collisions when the mass flow rate and the resulting neutral density are higher. Studying what determines the azimuthal distributions of the plasma flow and of the electric potential is a part of our research plan. We characterize the azimuthal uniformity by $u \equiv I_{per,2}/I_{av}$, the ratio of the minimal perpendicular ion current $I_{per,2}$ to the average perpendicular ion current $I_{av} = \Sigma_{j=1}^{4} I_{per,j}/4$. In Fig. 8, that ratio calculated for the data presented in Fig. 7 is shown to decrease as the mass flow rate increases. It is clear from Figs. 7 and 8 that in order to improve the uniformity, the RPS should be operated at a lower mass flow rate. At too small a mass flow rate, however, the discharge becomes unstable. Figure 9 shows the critical mass flow rate above which, for specified magnetic field intensity, the discharge is stable. The figure can be also viewed as showing the maximal magnetic field for which the discharge is stable for a specified mass flow rate.

We turn now to examine the influence of the magnetic field intensity on the RPS operation. Since we wanted the discharge to be stable for all values of the magnetic field intensity, we performed the measurements for a mass flow rate of 17.5 SCCM, the minimal mass flow rate for which the discharge was stable for 186 G, the highest magnetic field intensity that we employed. At that mass flow rate the gas pressure in the vacuum chamber was 2.5 mTorr. Figures 10–14 show how various discharge parameters vary as functions of the magnetic field intensity, all for 17.5 SCCM mass flow rate and 1.4 A discharge current. Again we first present in Fig. 10 the azimuthal uniformity measured by u as defined above. Here it is shown as a function of the magnetic field intensity.

In Fig. 11 the discharge voltage between the cathode and the anode is shown versus the magnetic field intensity. The discharge voltage is found to increase from 55 to 120 V with the increase in the magnetic field intensity from 0 up to 186 G. As expected, the increased magnetic field inhibits the electron cross-field mobility and therefore increases the volt-

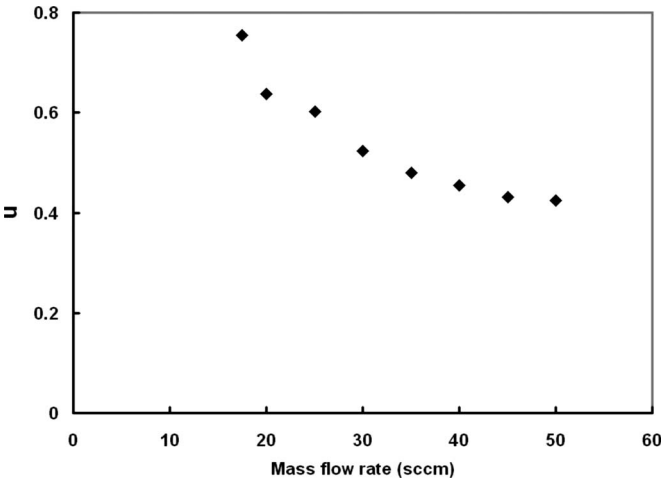

FIG. 8. The azimuthal uniformity as a function of the mass flow rate.

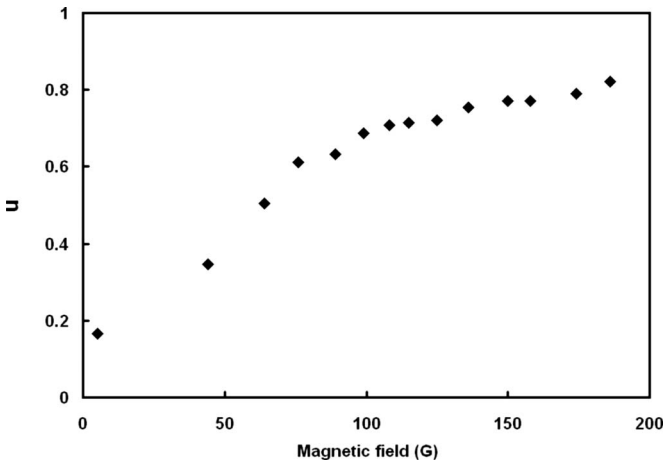

FIG. 10. The azimuthal uniformity as a function of the magnetic field intensity.

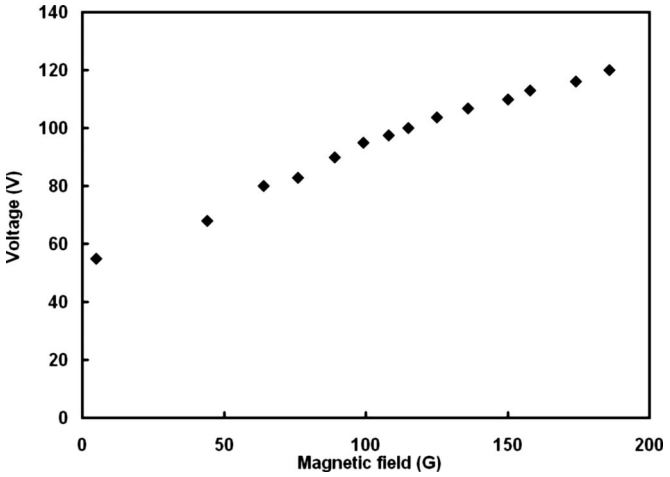

FIG. 11. The voltage between the cathode and the anode as a function of the magnetic field intensity.

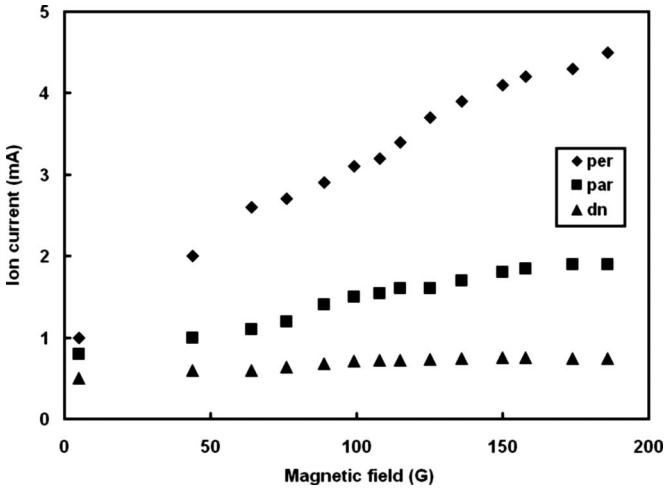

FIG. 13. The three different ion saturation currents (perpendicular, parallel, and downstream) measured in location 1 (Fig. 6) as functions of the magnetic field intensity.

age for the same specified discharge current. In order to obtain further information about the electric potential distribution between the cathode and the anode, we performed measurements with an emissive probe. The plasma potential was measured by the emissive probe outside the source at a distance of 5 cm from the source center. The emissive probe location is shown in Fig. 6. The emissive probe measurements presented in Fig. 12 show that the plasma potential at the probe location remains almost constant at a value of 30 V with respect to the cathode for all magnetic field intensities. The additional voltage drop, varied from 25 V in the absence of a magnetic field up to 90 V when the magnetic field is maximal, falls between the probe and the anode, probably where the axial magnetic field is present. Future measurements of the profile of the plasma potential between the anode and the cathode will be made by employing a movable emissive probe.

The measurements of the three different ion saturation currents into a Langmuir probe, as described in section II B, are shown in Fig. 13. The probe (denoted as 1 in Fig. 6) was located at the distance of 8 cm from the source center. Both I_{dn} and I_{par} weakly depend on the magnetic field intensity. The ion current I_{dn} varies from 0.6 to 0.75 mA while I_{par} varies from 1.05 to 1.5 mA when the maximal magnetic field intensity varies from 40 to 186 G. We assume that I_{dn} and I_{par} are proportional to nv_BS, where n is the plasma density, v_B is the Bohm velocity, and S is the collecting area. The collecting area is the probe area S_i for I_{dn} and $2S_i$ for I_{par}. The current I_{par} is then expected to be twice I_{dn}, as, indeed, it approximately is, according to Fig. 13.

Figure 13 also shows that while I_{dn} and I_{par} vary only weakly with the increase in the magnetic field intensity, the perpendicular ion current I_{per} increases significantly; it grows from 2 up to 4.5 mA when the magnetic field intensity is varied from 40 to 186 G, and the ratio $(I_{per}-I_{dn})/I_{dn}$ varies from 2.3 up to 5.1 for that change in the magnetic field intensity. The increase in the ratio indicates that the plasma flow velocity in the radial direction is supersonic.[15–19]

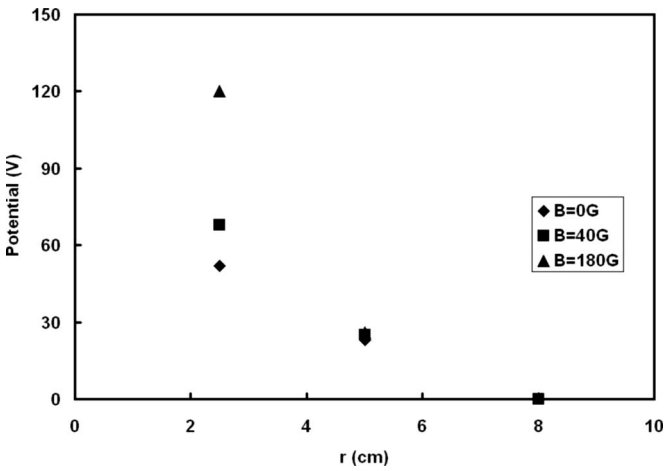

FIG. 12. The potential at $r=2.2$ cm (the anode) at $r=5$ cm (measured by the emissive probe, see Fig. 6) and at $r=8$ cm (the cathode) for three values of the magnetic field intensity.

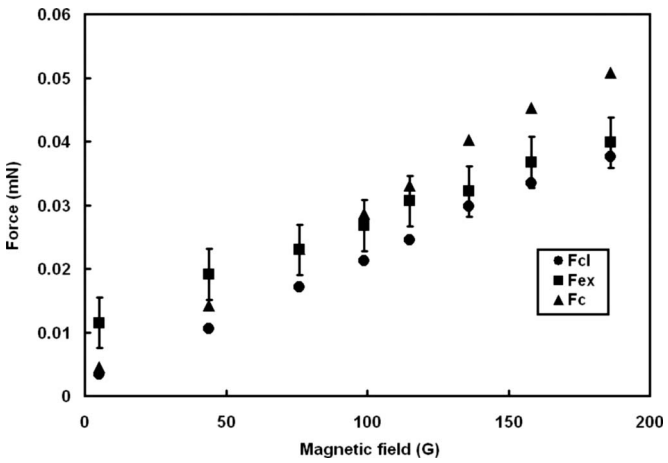

FIG. 14. The measured force F_{ex} [Eq. (1)] and the calculated forces F_{cl} [Eq. (12)] and F_c [Eq. (13)] as functions of the magnetic field intensity.

IV. THE FORCE EXERTED BY THE FLOW

The existence of a radial plasma flow that we concluded from the ion current measurements is confirmed by flow-force measurements described in the following. As described in Sec. II B we measured the force exerted on the flat plate of the balance force meter as a function of the magnetic field intensity when the flat plate was exposed to the plasma and was facing the center of the RPS. The measured force, calculated through Eq. (1), is shown in Fig. 14 and is denoted as F_{ex}. This is the net force exerted by the flow on the balance force meter, the difference between the two forces acting in opposite directions on the upstream and downstream sides of the balance force meter. The local force measurements were taken when the balance force meter was located at the position denoted as 1 in Fig. 6 at a distance of 8 cm from the plasma source center. As seen in Fig. 14, F_{ex} increases when the magnetic field increases.

We assume that the net force exerted by the flow on the balance force meter equals the net force exerted on the flow during its motion toward the balance force meter. The radial force exerted on the ions F_i and the radial force exerted on the neutrals F_N are, respectively,

$$F_i = neE - \nu_{iN} m_i n v, \quad F_N = \nu_{iN} m_i n v. \tag{3}$$

Here E is the radial electric field, e and m_i are the (singly ionized) ion charge and mass, v and n are the radial velocity and density of the ions, and ν_{iN} is the ion-neutral collision frequency. The total force exerted on the ion and neutral flow is therefore

$$F_i + F_N = neE. \tag{4}$$

The total force along the acceleration is

$$2\pi \int_{r_A}^{r_C} r(F_i + F_N) dr = 2\pi \int_{r_A}^{r_C} neErdr. \tag{5}$$

Let us assume that all the ionization occurs near the peak of the potential at the neighborhood of the anode, so that all ions are accelerated by the full voltage drop. We denote the (constant) ion flux by

$$\Gamma_i = 2\pi rbnv, \tag{6}$$

where b is the axial width of the flow. We assume that the flow does not expand axially much during the radial motion.

We examine now two opposite limits. At the limit that the ions are collisionless, the ion velocity is $v(r) = \sqrt{2e[V_a - V(r)]/m}$ and the plasma density is

$$n = \frac{\Gamma_i}{2\pi rb\sqrt{2e[V_a - V(r)]/m}}. \tag{7}$$

Here V_a is the discharge voltage and $V(r)$ is the potential with respect to the cathode at a distance r from the axis of the source. Substituting the expression for the density n into Eq. (5) and employing the relation $E = -\partial V/\partial r$, we obtain

$$2\pi b \int_{r_A}^{r_C} neErdr = e\Gamma_i \sqrt{\frac{2mV_a}{e}}. \tag{8}$$

At the collisionless limit all the momentum is delivered to the ions and none to the neutrals. At the collisional limit we assume that the electric force on the ions is balanced by the force exerted on them through collisions with neutrals

$$neE - \nu_{iN} mnv \approx 0. \tag{9}$$

Using $nv = \Gamma_i/(2\pi rb)$ and expressing the collision frequency as $\nu_{iN} = \sigma_{iN} v N$, where σ_{iN} is taken as constant, we write the electric force as

$$2\pi rbneE = \Gamma_i \sqrt{\sigma_{iN} N m_i e E}. \tag{10}$$

The total electric force is

$$2\pi b \int_{r_A}^{r_C} neErdr = \Gamma_i \sqrt{\sigma_{iN} Nme} \int_{r_A}^{r_C} dr\sqrt{E} \approx e\Gamma_i \sqrt{\frac{2mV_a}{e}} \sqrt{\frac{\sigma_{iN} Na}{2}}. \tag{11}$$

We approximated $V_a \approx Ea$ $(a \equiv r_C - r_A)$. The force exerted by the electric field is increased due to collisions by $\sqrt{a/(2\lambda)}$, where λ is the ion mean free path. This can be understood also as a result of slowing of the ions by collisions, and an increase in the time ions feels the electric field. Employing Eq. (9) and the approximated expressions for ν_{iN} and for V_a, we write the ion velocity as $v = \sqrt{eV_a/(2m)}\sqrt{2\lambda/a}$. From this expression we see that the ion velocity is reduced and the time the ion feels the electric field is increased both by $\sqrt{a/(2\lambda)}$.

We also calculate the ratio of the force to the power $e\Gamma_i V_a$. This ratio is $1/v = \sqrt{2m/(eV_a)}$ in the collisionless limit and $1/v = \sqrt{2m/(eV_a)}\sqrt{a/(2\lambda)}$ in the collisional limit. We note that the form of the force increase would be different if, for example, the collision frequency, rather than the cross section, would be constant.

We turn now to calculate the force that is expected to be exerted on the balance force meter. We assume that ions and neutrals lose all their momenta to the balance force meter upon colliding with it. Employing expression (8), we find that the force exerted on the balance force meter if ions are collisionless is

$$F_{cl} = \frac{S_F}{S_i} I_i \frac{m}{e} \sqrt{\frac{2eV_a}{m}}, \tag{12}$$

where S_F and S_i are the areas of the balance force meter and the flat Langmuir probe, respectively, and $I_i \equiv I_{per} - I_{dn}$. As mentioned above, the measured force exerted on the balance force meter is shown in Fig. 14. The force F_{cl}, calculated with the measured I_i and V_a, is also shown as a function of the magnetic field in Fig. 14. As the measured force, the force F_{cl} also increases with the increase in the magnetic field intensity. However, F_{cl} is *smaller* than F_{ex} (although the difference is smaller for a higher magnetic field). Collisions of the accelerated ions increase the force exerted on the balance force meter. The maximal force can be estimated from expression (11),

$$F_c = \frac{S_F}{S_i} I_i \frac{m}{e} \sqrt{\frac{2eV_a}{m}} \sqrt{\frac{a}{2\lambda}}. \quad (13)$$

Again, the force in the collisional case F_c is larger than the force in the collisionless case F_{cl} by $\sqrt{a/(2\lambda)}$ for the same ion current and discharge voltage.

The calculated F_c for our experiment is shown in Fig. 14. It is seen to be *larger* than F_{ex} for the higher values of the magnetic field intensity. This disparity indicates that a considerable part of the force is exerted by the neutral gas, which has gained momentum from the plasma via ion-neutral collisions. The force is increased because the momentum delivered for a given deposited power is larger if the energy is deposited in a larger mass, as happens here through plasma collisions.

The measured force is larger than F_{cl} probably because of collisions. It is easy to show that that increase in force is only by collisions in the acceleration region, where the electric field is present. For a higher magnetic field the acceleration is concentrated in the vicinity of the anode probably in the magnetized region. The effective ratio of the acceleration length to the mean free path is smaller than a/λ. This effective ratio becomes even smaller when the magnetic field is increased so that the effect of collisions becomes smaller. We suggest that this is the reason that the measured force F_{ex} is closer to F_{cl} when the magnetic field is high.

At the opposite limit of low values of the magnetic field the discharge is not uniform and the measured force is larger than both F_{cl} and F_c. This regime requires a further study.

V. SUMMARY

We described the properties of the plasma generated by a RPS immersed in an applied radial electric field and axial magnetic field. The ion saturation currents into a Langmuir probe have been measured as functions of the argon-gas mass flow rate and of the magnetic field intensity. In addition, we examined the influence of the magnetic field intensity on the discharge voltage and on the voltage drop in the anode vicinity. The variations in the azimuthal uniformity and in the voltage have been discussed. The force exerted by the flow on a balance force meter has been found to be larger than the force exerted by the plasma flow. This disparity indicates that a considerable part of the force is exerted by the neutral gas, which has gained momentum from the plasma via ion-neutral collisions. The force is increased because the momentum delivered for a given deposited power is larger if the energy is deposited in a larger mass, as happens here through plasma collisions.

We will continue the study of the plasma flow in the crossed electric and magnetic fields of the RPS. Among the planned measurements, we will measure in the future the various plasma parameters for various values of the discharge current. We will also measure the force in different distances from the axis of the source.

ACKNOWLEDGMENTS

The authors wish to thank Dr. Y. Raitses and Professor N. J. Fisch for helpful comments. This research has been partially supported by the Israel Science Foundation (Grant No. 864/07).

[1] I. I. Beilis, R. L. Boxman, S. Goldsmith, and V. L. Paperny, Appl. Phys. Lett. **75**, 2734 (1999).
[2] A. Goncharov and I. Brown, IEEE Trans. Plasma Sci. **32**, 80 (2004).
[3] G. A. Pozdnyakov, Tech. Phys. Lett. **33**, 474 (2007).
[4] M. Rondanini, C. Cavallotti, D. Ricci, D. Chrastina, G. Isella, T. Moiseev, and H. von Kanel, J. Appl. Phys. **104**, 013304 (2008).
[5] B. Alterkop, E. Gidalevich, S. Goldsmith, and R. L. Boxman, J. Phys. D **41**, 105211 (2008).
[6] A. I. Morozov, Yu. V. Esipchuk, G. N. Tilinin, A. V. Trofimov, Yu. A. Sharov, and G. Ya. Smirnov, Sov. Phys. Tech. Phys. **17**, 54 (1972).
[7] L. B. King and A. D. Gallimore, Rev. Sci. Instrum. **68**, 1183 (1997).
[8] D. G. Chavers and F. R. Chang-Diaz, Rev. Sci. Instrum. **73**, 3500 (2002).
[9] A. Fruchtman, Plasma Sources Sci. Technol. **17**, 024016 (2008).
[10] D. G. Dimitriu, M. Aflori, L. M. Ivan, C. Ionita, and R. W. Schrittwieser, Plasma Phys. Controlled Fusion **49**, 237 (2007).
[11] R. Stenzel, C. Ionita, and R. Schrittwieser, IEEE Trans. Plasma Sci. **36**, 1000 (2008).
[12] S. A. Cohen, F. Zonca, J. Timberlake, T. Bennett, J. Cuthbertson, W. Langer, and R. Motley, Rev. Sci. Instrum. **61**, 3586 (1990).
[13] N. Hershkowitz and N. M. Cho, J. Vac. Sci. Technol. A **6**, 2054 (1988).
[14] Y. Raitses, D. Staack, A. Smirnov, and N. J. Fisch, Phys. Plasmas **12**, 073507 (2005).
[15] L. Oksuz and N. Hershkowitz, Plasma Sources Sci. Technol. **13**, 263 (2004).
[16] M. Hudis and L. M. Lidsky, J. Appl. Phys. **41**, 5011 (1970).
[17] I. H. Hutchinson, Phys. Plasmas **9**, 1832 (2002).
[18] N. Hershkowitz and L. Oksuz, Phys. Plasmas **9**, 1835 (2002).
[19] S. Shinohara, Phys. Plasmas **9**, 1834 (2002).